JOC Articles

Chemistry of Pyrrolo[1,2-*a*]indole- and Pyrido[1,2-*a*]indole-Based Quinone Methides. Mechanistic Explanations for Differences in Cytostatic/Cytotoxic Properties

Omar Khdour and Edward B. Skibo*

Department of Chemistry and Biochemistry, Arizona State University, Tempe, Arizona 85287-1604

eskibo@asu.edu

Received May 3, 2007

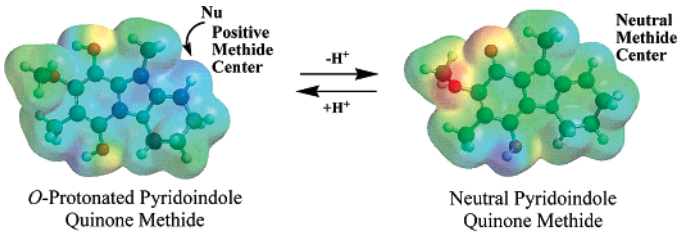

O-Protonation required for nucleophile trapping.

In the present study we investigate pyrido[1,2-*a*]indole- and pyrrolo[1,2-*a*]indole-based quinones capable of forming quinone methide and vinyl quinone species upon reduction and leaving group elimination. Our goals were to determine the influence of the 6-membered pyrido and the 5-membered pyrrolo fused rings on quinone methide and vinyl quinone formation and fate as well as on cytostatic and cytotoxic activity. We used the technique of Spectral Global Fitting to study the fleeting quinone methide intermediate directly. Conclusions regarding quinone methide reactivity are that carbonyl *O*-protonation is required for nucleophile trapping and that the pK_a value of this protonated species is near neutrality. The abnormally high protonated carbonyl pK_a values are due to the formation of an aromatic carbocation species upon protonation. The fused pyrido ring promotes quinone methide and vinyl quinone formation but slows nucleophile trapping compared to the fused pyrrolo ring. These findings are explained by the presence of axial hydrogen atoms in the fused pyrido ring resulting in more steric congestion compared to the relatively flat fused pyrrolo ring. Consequently, pyrrolo[1,2-*a*]indole-based quinones exhibit more cytostatic activity than the pyrido[1,2-*a*]indole analogues due to their greater nucleophile trapping capability.

Introduction

Herein we report on our continuing efforts to design and study alkylating species activated by cellular quinone reduction.[1−12] This "bioreductive alkylation" process, first proposed by Moore for quinone natural products,[13,14] has become important in cancer drug design. The success of bioreductive alkylation is largely

* Address correspondence to this author. Phone: 480-965-3581. Fax: 480-965-2747.

(1) Skibo, E. B. *J. Org. Chem.* **1986**, *51*, 522−527.
(2) Lee, C.-H.; Skibo, E. B. *Biochemistry* **1987**, *26*, 7355−7362.
(3) Lemus, R. L.; Skibo, E. B. *J. Org. Chem.* **1988**, *53*, 6099−6105.
(4) Lemus, R. L.; Lee, C. H.; Skibo, E. B. *J. Org. Chem.* **1989**, *54*, 3611−3618.
(5) Islam, I.; Skibo, E. B. *J. Org. Chem.* **1990**, *55*, 3195−3205.
(6) Islam, I.; Skibo, E. B.; Dorr, R. T.; Alberts, D. S. *J. Med. Chem.* **1991**, *34*, 2954−2961.
(7) Skibo, E. B. *J. Org. Chem.* **1992**, *57*, 5874−5878.
(8) Skibo, E. B.; Schulz, W. G. *J. Med. Chem.* **1993**, *36*, 3050−3055.
(9) Schulz, W. G.; Islam, E.; Skibo, E. B. *J. Med. Chem.* **1995**, *38*, 109−118.
(10) Schulz, W. G.; Nieman, R. A.; Skibo, E. B. *Proc. Natl. Acad. Sci. U.S.A.* **1995**, *92*, 11854−11858.
(11) Skibo, E. S.; Gordon, S.; Bess, L.; Boruah, R.; Heileman, J. *J. Med. Chem.* **1997**, *40*, 1327−1339.
(12) Khdour, O.; Ouyang, A.; Skibo, E. B. *J. Org. Chem.* **2006**, *71*, 5855−5863.
(13) Moore, H. W. *Science* (*Washington, D.C.*) **1977**, *197*, 527−532.
(14) Moore, H. W.; Czerniak, R. *Med. Res. Rev.* **1981**, *1*, 249−280.

10.1021/jo070866o CCC: $37.00
Published on Web 10/10/2007

CHART 1. Reductive Activation and Double Leaving Group Elimination

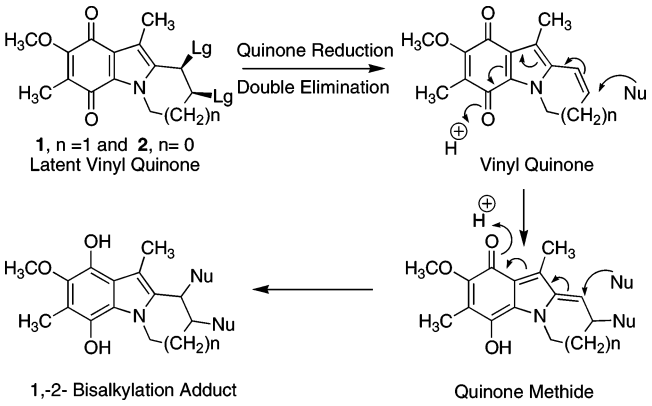

CHART 2. Reductive Activation and Single Leaving Group Elimination

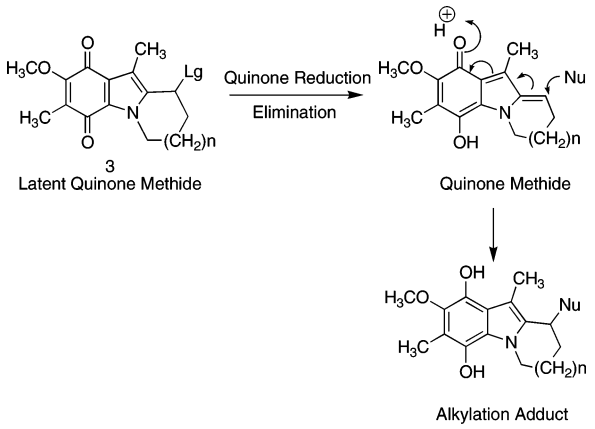

due to the expression of the 2-electron reducing enzyme DT-diaphorase in some histological cancer types.[15−19] In the present study we compare the reductive activation of pyrido[1,2-*a*]indole (**2**, $n = 1$) and pyrrolo[1,2-*a*]indole (**1**, $n = 0$) based quinones (Chart 1). Our goals were to determine the influence of the 6-membered pyrido and the 5-membered pyrrolo fused rings on quinone methide and vinyl quinone and formation as well as cytostatic/cytotoxic activity. We developed a new technique for rapid quinone reduction to the hydroquinone in a Thunberg (anaerobic) cuvette. As a result, it was possible to carry out direct kinetic studies of quinone methide formation and fate by using Spectral Global Fitting.[20] The postulate made at the outset of this study was that reactive species derived from the 6-membered pyrido ring analogues would be less reactive than those derived from the 5-membered pyrrolo ring analogues. The presence of axial hydrogens in the fused pyrido ring, in contrast to the relatively flat fured pyrrolo ring, was the basis for this postulate. The results of this study would provide an explanation of the prevalence of the pyrrolo[1,2-*a*]indole system in naturally occurring bioreductive alkylating agents, e.g., the mitomycins and mitosenes.[21]

Chart 1 shows the pyrido[1,2-*a*]indole- and pyrrolo[1,2-*a*]-indole-based latent vinyl quinone systems **1** and **2**, which upon reduction and elimination of both leaving groups could afford the vinyl quinone species. The consecutive addition of two nucleophiles to the vinyl quinone, via a quinone methide intermediate, will afford a 1,2-bisalkylation adduct. Therefore the vinyl quinone species could be a 1,2-bisalkylator and as a result possess antitumor activity. Previously, the reactive vinyl quinone species has been used as a synthetic intermediate as well as a monomer.[22−26] In addition, vinyl quinone systems have been proposed by Moore to be the Michael acceptors formed upon reductive activation and leaving group elimination from naturally occurring quinones.[13] On the basis of our initial postulate, we expected the vinyl quinone formation to be favored in the pyrido-fused system **1**, but not in the pyrrolo-fused system **2**. Steric congestion in the latter system was expected to favor the elimination reactions leading to double bond formation.

Chart 2 shows the pyrido[1,2-*a*]indole- and pyrrolo[1,2-*a*]-indole-based latent quinone methide systems **3**. Reduction of **3** to the hydroquinone followed by leaving group elimination would afford the pyrido- and the pyrrolo-fused quinone methides. The plan was to carry out kinetic studies, calculations, and cytostatic/cytotoxic determinations on **3** to assess the influence ring size has on chemical and biological properties. The results of these studies would have a bearing on the documented lack of antitumor activity exhibited by pyrido[1,2-*a*]indole analogues[27] as well as the activity of the pyrrolo[1,2-*a*]indole-based antitumor agents.

Results and Discussion

Synthesis. The synthesis of the pyrido[1,2-*a*]indole-based latent vinyl quinone system **1** is outlined in Schemes 1 and 2. The preparation of the racemic cis-diol key intermediate **8** (Scheme 1) was carried out starting with ketone **4** that was previously prepared in the laboratory.[12] Reduction of the ketone group of **4** to an alcohol with sodium borohydride was followed by treatment with methanesulfonyl chloride/DMAP to afford **6** in a one-pot reaction. The racemic cis-diol **7** was conveniently obtained by catalytic osmium tetroxide oxidation of **6** with *N*-methylmorpholine *N*-oxide to regenerate the oxidizing agent. Catalytic reduction of the nitro group of **7** to an amine followed by Fremy oxidation[28] of the resulting amine afforded a mixture of quinone **8** and iminoquinone **9**. The iminoquinone **9** is the actual product of Fremy oxidation that hydrolyses to the quinone in acidic media. We have previously prepared iminoquinones by the Fremy oxidation of aromatic amines in neutral buffers.[5]

Scheme 2 shows the reactions affording the various analogues of **1** used in mechanistic and cytotoxic studies. Acetylation of **8** with acetic anhydride in the presence of DMAP affords the

(15) Gutierrez, P. L. *Free Radical Biol. Med.* **2000**, *29*, 263−275.
(16) Rauth, A. M.; Goldberg, Z.; Misra, V. *Oncol. Res.* **1997**, *9*, 339−349.
(17) Garrett, M. D.; Workman, P. *Eur. J. Cancer* **1999**, *35* (14), 2010−2030.
(18) Stratford, I. J.; Workman, P. *Anti-Cancer Drug. Des.* **1998**, *13*, 519−528.
(19) Workman, P. *Oncol. Res.* **1994**, *6*, 461−475.
(20) Beecham, J. M.; Brand, L. *Photochem. Photobiol.* **1986**, *44*, 323−329.
(21) Tomasz, M.; Palom, Y. *Pharmacol. Ther.* **1997**, *76*, 73−87.
(22) Parker, K. A.; Mindt, T. L. *Org. Lett.* **2001**, *3*, 3875−3878.
(23) Parker, K. A.; Ruder, S. M. *J. Am. Chem. Soc.* **1989**, *111*, 5948−5949.
(24) Parker, K. A.; Mindt, T. L. *Org. Lett.* **2002**, *4*, 4265−4268.
(25) Germeraa, P.; Moore, H. W. *J. Org. Chem.* **1974**, *39*, 774−780.
(26) Irngartinger, H.; Lichtenthaler, J.; Herpich, R.; Stadler, B. *Mol. Cryst. Liq. Cryst. Sci. Technol., Section a. A* **1996**, *276*, 349−360.
(27) Orlemans, E. O. M.; Verboom, M. W.; Scheltinga, M. W.; Reinhoudt, D. N.; Lelieveld, P.; Fiebig, H. H.; Winterhalter, B. R.; Double, J. A.; Bibby, M. C. *J. Med. Chem.* **1989**, *32*, 1612−1620.
(28) Zimmer, H.; Lankin, D. C.; Horgan, S. W. *Chem. Rev.* **1971**, *71*, 229−246.

SCHEME 1. Preparation of 8 and 9

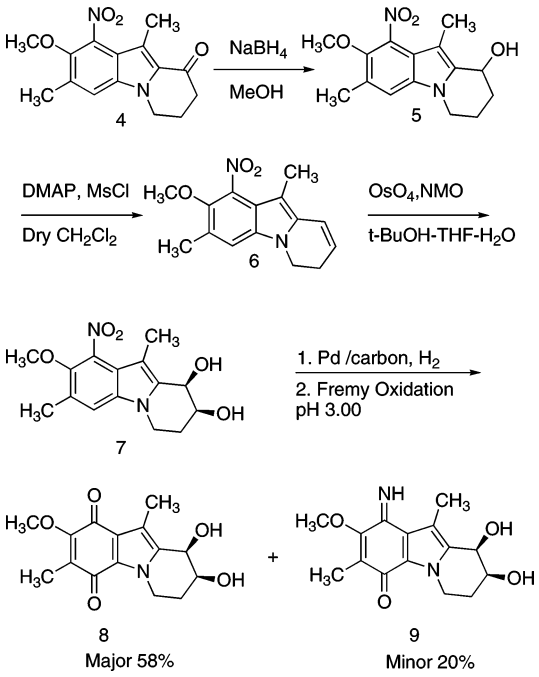

SCHEME 2. Preparation of Analogues of 1

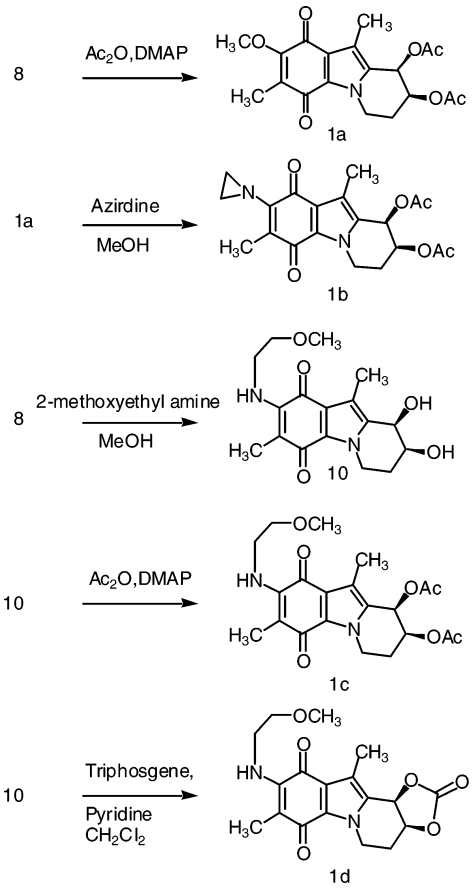

desired *cis*-diacetate **1a**. Aziridination of **1a** in methanol afforded **1b**, which is a potential triple alkylating agent with high cytotoxic activity. However, the presence of an electron-rich amine substituent would influence quinone methide fate by favoring proton trapping over nucleophile trapping. The mechanistic study of **1c** would serve to confirm quinone methide

SCHEME 3. Preparation of Cis/Trans 16

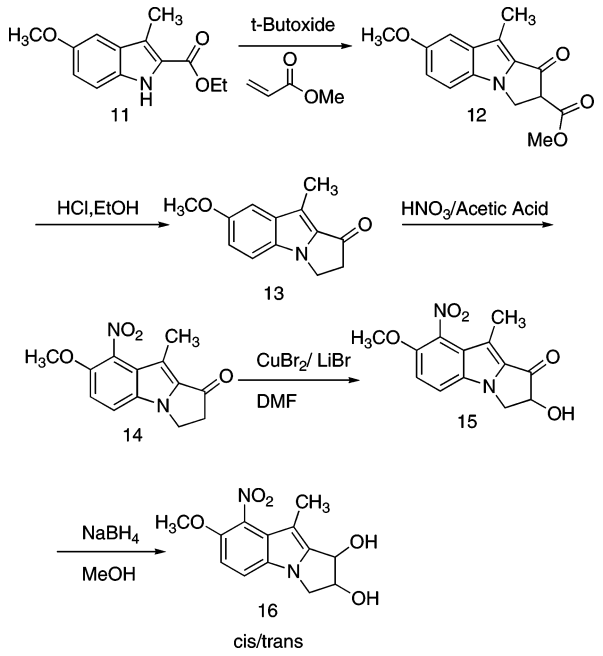

SCHEME 4. Preparation of Analogues of 2

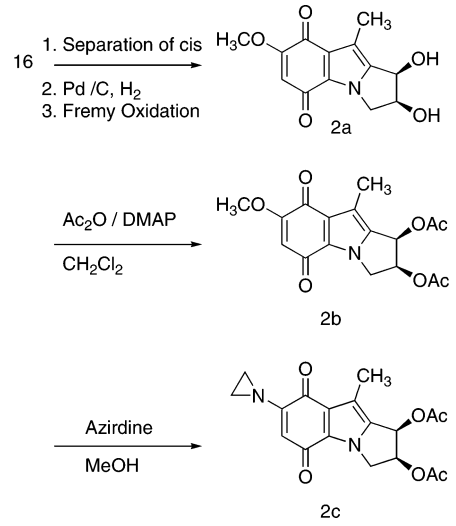

formation. The preparation of **1c** involved the treatment of **8** with 2-methoxyethylamine followed by treatment of the product **10** with an excess of acetic anhydride. The cyclic carbonate leaving group of **1d** was prepared by treating **10** with triphosgene.

The synthesis of the pyrrolo[1,2-*a*]indole-based latent vinyl quinone system **2** is outlined in Schemes 3 and 4. The synthetic steps leading to series **2** are based on previous reports from this laboratory[29] and elsewhere.[30] Annelation of the pyrrolo ring was carried out by treatment of **11**[31] with methyl acrylate in the presence of potassium *tert*-butoxide. The annelation product **12** was decarboxylated to **13**, which was then nitrated to afford **14**. Treatment of **14** with cupric bromide/lithium bromide in DMF afforded a mixture of products including 2-bromo,

(29) Boruah, R. C.; Skibo, E. B. *J. Med. Chem.* **1994**, *37*, 1625−1631.
(30) Allen, G. R., Jr.; Poletto, J. C.; Weiss, M. J. *J. Org. Chem.* **1965**, *30*, 2897−2904.
(31) Zhao, S.; Liao, X.; Wang, T.; Flippen-Anderson, J.; Cook, J. M. *J. Org. Chem.* **2003**, *68*, 6279−6295.

SCHEME 5. Preparation of Analogues of 3

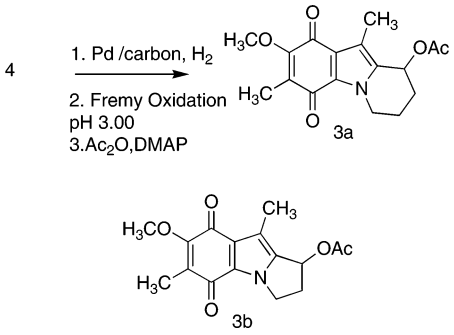

2-hydroxy, and 2-formyloxy derivatives. Aqueous acid workup afforded the desired 2-hydroxy derivative **15**. Borohydride reduction of **15** afforded the diol **16** as a cis/trans mixture. Chromatographic separation afforded the cis isomer that was identified with 2d H NMR. Quinone elaboration from *cis*-**16** to afford **2a** was carried out by nitro group reduction followed by Fremy oxidation. Other analogues of **2** required for the present study were prepared as shown in Scheme 5.

The monosubstituted analogue **3a** was prepared from **4** as shown in Scheme 5. Compound **3b** was prepared as previously described.[29]

Products of Reductive Activation. The product studies described below provided circumstantial evidence of the formation of quinone methide species upon the reductive activation of **1a**, **1c**, **2b**, **3a**, and **3b**. These quinone methide species can trap a nucleophile (methanol or water) and an electrophile (proton). Much of the earlier quinone methide literature has documented nucleophile and proton trapping reactions.[32−35] In addition, some quinone methides discussed in this report can form a vinyl quinone by elimination of a second leaving group. Finally, the vinyl quinone product can undergo prototropic reactions to afford an aromatized product as well as other structurally novel products. Scheme 6 shows the structures of isolated products resulting from the reductive activation of **1a** in anaerobic aqueous buffer (phosphate, pH 7.4) and in anaerobic methanol. Scheme 7 shows the structures of isolated products resulting from the reductive activation of the electron-rich analogue **1c** in anaerobic aqueous buffer (phosphate, pH 7.4). The mechanisms associated with the formation of these isolated products are discussed in conjunction with Schemes 8−13.

Reduction of **1a** in anaerobic pH 7.4 phosphate buffer affords **17** in high yield along with minor amounts of **18**. Inspection of the anaerobic reaction mixture before aerobic workup revealed the presence of the red chromophore associated with **17**. Therefore, **17** was formed by the double elimination process shown in Scheme 8 rather than by oxidation upon aerobic workup. The vinyl quinone species **17** can undergo aromatization to **18H$_2$**, which upon air oxadation affords the blue aromatized quinone **18**. Our calculations (Hartree−Fock calculations were carried out with the 3-21G(*) basis set)[36] show that the aromatization of **17** is favorable by 6 kcal/mol. Shown

SCHEME 6. Products Resulting from the Reductive Activation of 1a

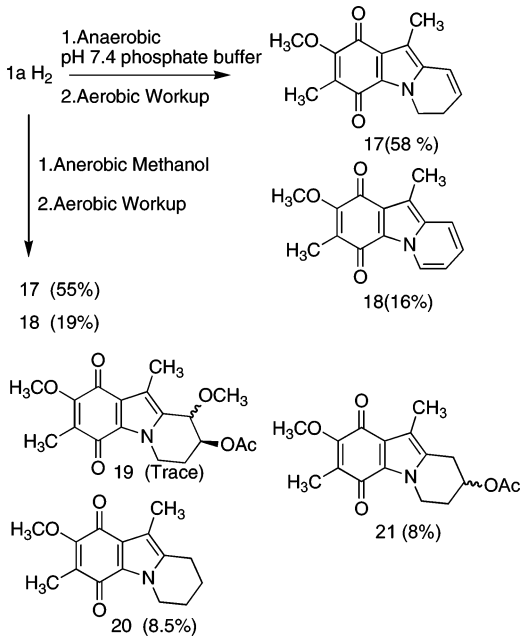

SCHEME 7. Products Resulting from the Reductive Activation of 1c

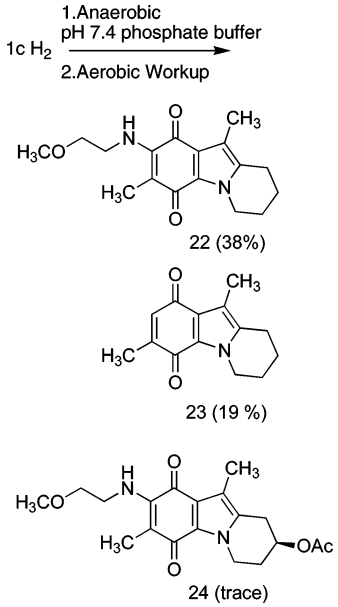

in Scheme 9 is the mechanism for aromatization via two prototropic shifts and the calculated relative energies of the reacting intermediates. Although aromatization is energetically favored, the presence of a relatively high-energy intermediate tautomer (labeled 0 kcal/mol) precludes the complete conversion to the aromatized product.

Reduction of **1a** in anaerobic methanol also affords **17** in high yield upon aerobic workup along with minor amounts of **18**. We also isolated and identified trace amounts of **19**−**21** in this reaction. The presence of **19** and **21** supports a quinone methide intermediate that traps methanol and a proton to afford these respective products, see Scheme 8 for mechanisms. We

(32) Bird, D. M.; Gaudiano, G.; Koch, T. H. *J. Am. Chem. Soc.* **1991**, *113*, 308−315.

(33) Taatjes, D. J.; Gaudiano, G.; Resing, K.; Koch, T. H. *J. Med. Chem.* **1996**, *39* (21), 4135−4138.

(34) Pande, P.; Shearer, J.; Yang, J. H.; Greenberg, W. A.; Rokita, S. E. *J Am. Chem. Soc.* **1999**, *121*, 6773−6779.

(35) Rokita, S. E.; Yang, J. H.; Pande, P.; Greenberg, W. A. *J. Org. Chem.* **1997**, *62*, 3010−3012.

(36) Durig, J. R.; Berry, R. J.; Durig, D. T.; Sullivan, J. F.; Little, T. S. *Teubner-Texte Phys.* **1988**, *20*, 54−68.

SCHEME 8. Mechanisms of Product Formation upon Reductive Activation

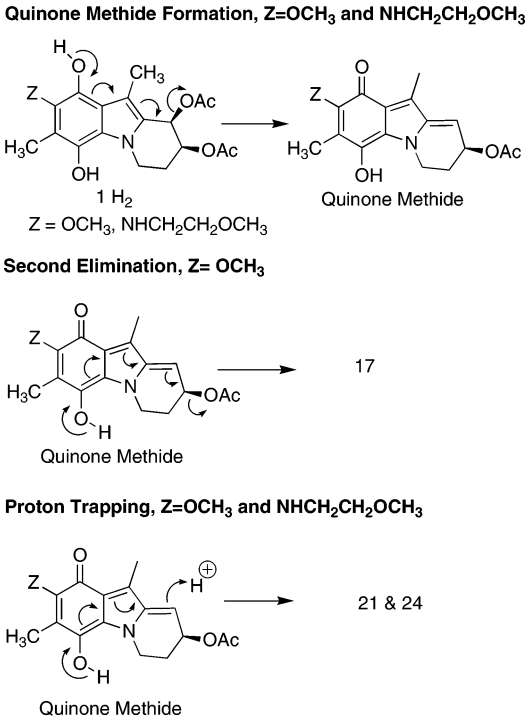

SCHEME 9. Aromatization Mechanism

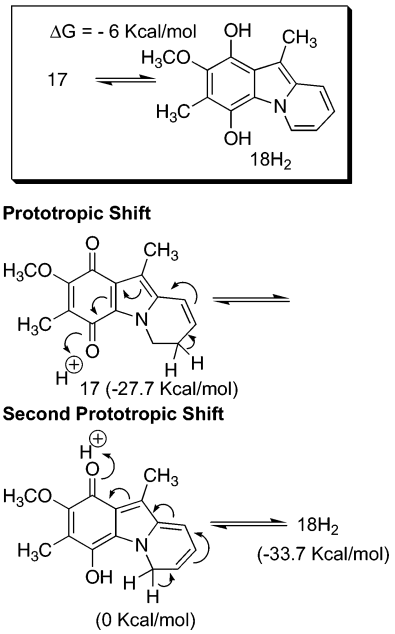

attribute the formation of **20** to an internal redox reaction wherein the hydroquinone ring transfers electrons to the double bond of the fused pyrido ring by means of prototropic shifts (see the mechanism in Scheme 10). Although **20** was isolated upon aerobic workup, this compound very likely arises while the reaction mixture is anaerobic (see the mechanism in Scheme 10).

The internal redox reaction that affords **20** in trace amounts becomes the predominate process upon reductive activation of analogue **1c** (see Scheme 7 for product structures). The presence of the amino substituent of **1c** results in an excessively electron-rich hydroquinone ring that favors the observed internal redox

SCHEME 10. Internal Redox Mechanisms

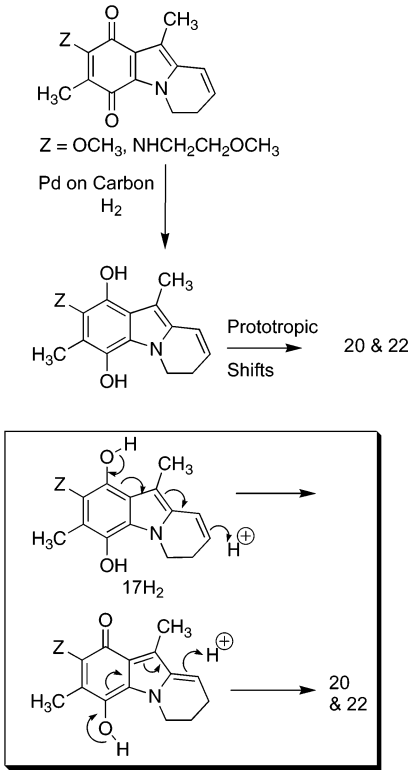

SCHEME 11. Reductive Elimination Mechanism

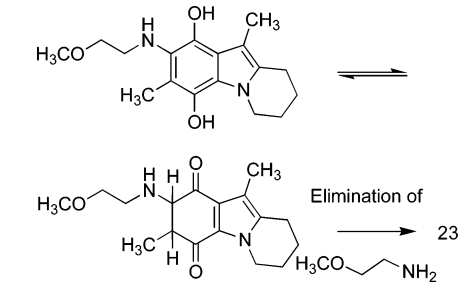

reaction. The excessively electron-rich hydroquinone ring also favors hydroquinone tautomerization and amine elimination to afford **23** as illustrated in Scheme 11.

The double elimination reaction did not occur upon reductive activation of **2b**, although an analogue of the pyrroloindole vinyl quinone has been reported in the literature.[37] The major observed product is the quinone methide water-trapping product, **25** (Scheme 12). The proton-trapping product **26** was observed in only trace amounts. Apparently the rapid trapping of the quinone methide intermediate by water prevented the second acetate elimination.

The apparent stability of **17**, judging from its ease of synthesis and stability in solution, suggests that it would not be an effective double alkylating agent. The reaction of **17** with ethylene diamine in methanol merely resulted in displacement of the methoxy group followed by cyclization to afford **27**. The LUMO of **17** shows high coefficient values in the quinone ring where nucleophilic attack and displacement actually occur. In contrast, the alkene center has a negligible wave function coefficient indicating that nucleophile attack is not likely at this

(37) Naruta, Y.; Nagai, N.; Maruyama, K. *J. Chem. Soc., Perkin Trans. 1* **1988**, 1143−8.

SCHEME 12. Products of 2b Reductive Activation

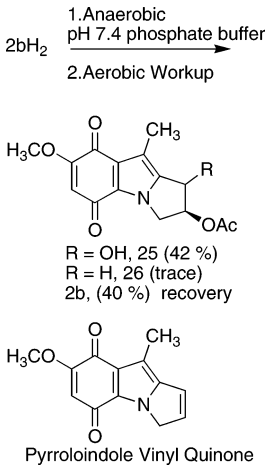

SCHEME 13. Nucleophilic Trapping Product of 17 and the LUMO of 17

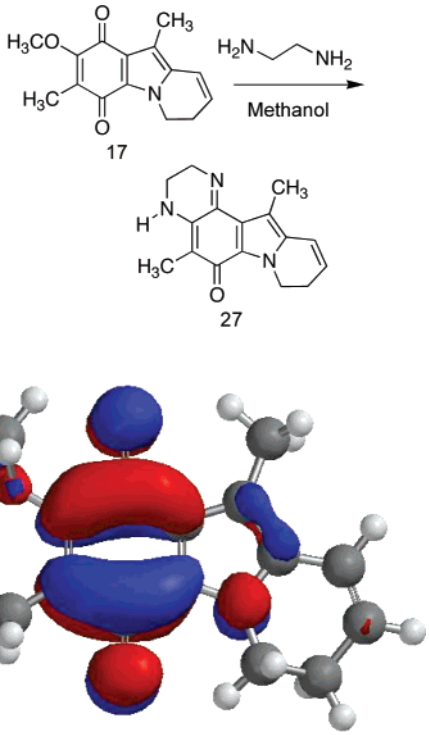

center. Consistent with the presence of an alkylation reaction involving the quinone ring, **17** possesses modest cytostatic activity.

Quinone Methide Formation and Fate and Reaction Kinetics. The goal of these studies was to determine the reactivity differences between the pyrroloindole and pyridoindole quinone methides by using product studies, kinetic studies, and calculations.

The results of the isolation studies are shown in Scheme 14. The dominant quinone methide reaction path for the pyrroloindole quinone methide system at pH 7.4 and 5.0 is the nucleophilic trapping of water. In contrast, the pyridoindole quinone methide undergoes significant prototropic reactions along with the nucleophilic trapping water, particularly at the pH values of 7.4 and 5. At pH 9.0 the pyridoindole quinone methide only traps water.

SCHEME 14. Products of 3a,b Reductive Activation

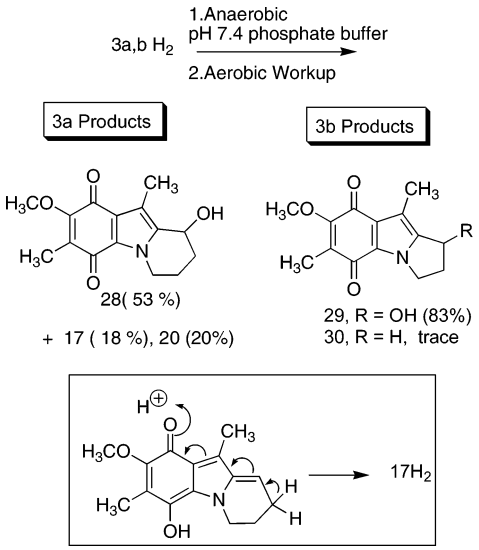

The kinetic study of quinone methide formation and fate is difficult because of the presence of two transient species, the hydroquinone and quinone methide. Although these species possess different UV−visible spectra, absorbance vs time measurements at a single wavelength may not provide rate constant data for both of these reacting species. To carry out this kinetic study we used Spectral Global Fitting, a technique that has been used to visualize and study photochemical intermediates.[20,38] Spectral Global Fitting involves repetitive UV−visible scanning of reaction mixtures with time resulting in a surface showing spectral changes associated with the reaction. Fitting the entire range of wavelengths (Global Fitting) to a rate law provides accurate rate constants and intermediate spectra associated with the reaction under study. We recently reported the use of Spectral Global Fitting to study a transient intermediate involved in CC-1065 A-ring opening.[39]

To generate the hydroquinone form of **3a**,**b** in an anaerobic atmosphere, we utilized a Thunberg cuvette with a quinone DMSO stock solution in the top port and a buffer solution containing suspended 5% Pd on Carbon in the bottom port. The cuvette was purged with hydrogen and sealed. The reduction reaction was initiated by mixing the ports. Repetitive UV−visible scanning of the reaction with time afforded an absorbance vs time vs wavelength surface, an example of which is shown in Figure 1. The reduction reaction is fast and is complete in a single scan (∼2 min). The surface shown in Figure 1 was obtained with 4-fold less catalyst than is used for kinetic studies so that the initial quinone spectrum can be observed. Global fitting of the entire surface to a three-exponential rate law (Abs $= Ae^{-kt} + Be^{-k't} + Ce^{-k''t} + D$) afforded the three rate constants associated with quinone methide formation from the hydroquinone (k_{obsd}), quinone methide disappearance (k'_{obsd}), and the slow precipitation of the finally divided catalyst (k''_{obsd}). In this rate law Abs refers to the total absorbance at a given time and wavelength and constants $A-D$ refer to the absorbance at this wavelength for each reacting species. In all reactions, the relative magnitude of rate constants was quinone methide formation > quinone methide disappearance ≫ catalyst precipitation. Some

(38) Matheson, I. B. C. *Anal. Instrum.* **1987**, *16*, 345−373.
(39) LaBarbera, D. V.; Skibo, E. B. *J. Am. Chem. Soc.* **2006**, *128*, 3722−3727.

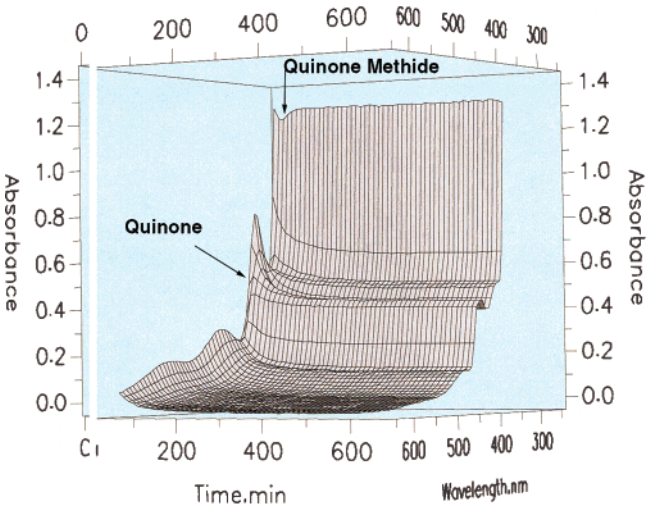

FIGURE 1. Surface produced by reduction of **3a** in anaerobic 0.2 M pH 8.5 boric acid buffer at 30 °C. The reaction mixture was repetitively scanned 100× from 240 to 600 nm.

reactions exhibited rapid quinone methide formation and we fit the surface to a two-exponential rate law (Abs = $Ae^{-k't} + Be^{-k''t} + C$). We should point out that fits to three-exponential rate laws could provide solutions that are not unique. However, fitting each wavelength from 240 to 600 nm to the same rate law will provide a unique solution. We also should point out that casual inspection of the surface shown in Figure 1 does not show the obvious buildup of a quinone methide species (see quinone methide arrow in this figure). The Spectral Global Fitting over the wavelength range studied requires the buildup of such a transient species early in the reaction.

Equation 1 gives the rate law for quinone methide formation

$$k_{obsd} = a_H k_1 + k_0$$

and eq 2 gives the rate law for quinone methide disappearance.

$$k'_{obsd} = \frac{(a_H k_2 + K_w[k_3 + k_4])}{(a_H + K_a)}$$

In Scheme 15, we outline the proposed mechanism for quinone methide formation and disappearance based on the studies presented below. Global fitting provided the rates of quinone methide formation from the hydroquinone forms of **3a**,**b** that are plotted as log k_{obsd} vs pH in Figure 2. The rate constants associated with the conversion of reduced **3b** to its quinone methide were fit to the rate law in eq 1. The solid line was generated with eq 1 where $k_0 = 0.09$ min^{-1} and $k_1 = 1.5 \times 10^5$ M^{-1} min^{-1}. The mechanism consistent with the pH−rate profile for reduced **3b** is the spontaneous elimination of acetate (k_0 process) and the proton assisted elimination of acetate (k_1 process) from the electron-rich hydroquinone. The k_0 process is independent of pH and exhibits a zero slope while the k_1 process exhibits a −1 slope consistent with acid catalysis. The rate constants associated with the acid-catalyzed conversion of reduced **3a** to its quinone methide were too large to measure. We did manage to measure two rate constants at pH 7 and 8, both with a value of 0.36 min^{-1}. On the basis of the pH−rate profile obtained for reduced **3b**, these rate constants very likely represent the k_0 process of reduced **3a**. Even with two data

SCHEME 15. Quinone Methide Formation and Fate

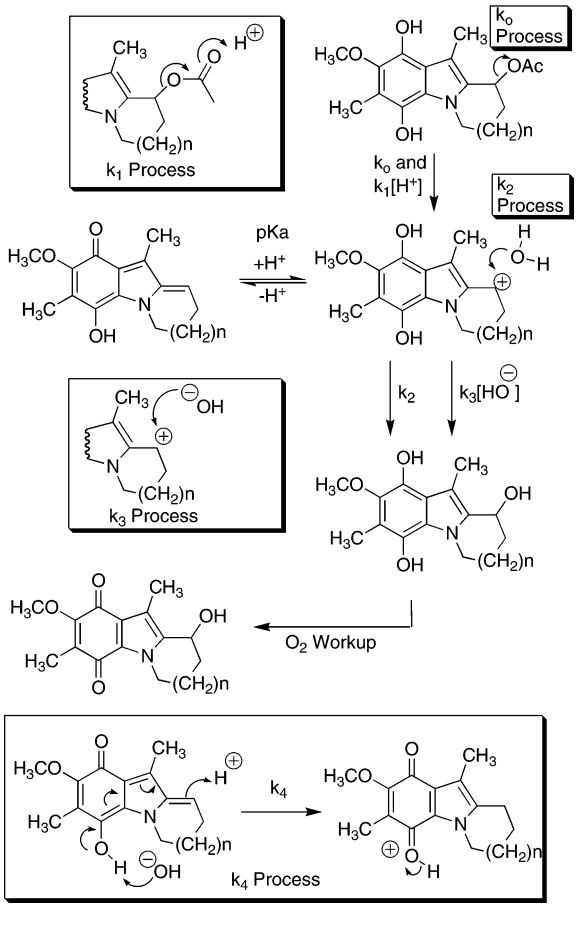

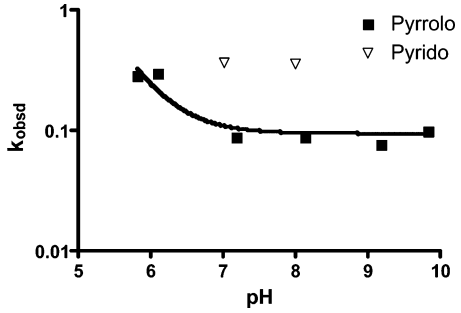

FIGURE 2. pH−rate profile for quinone methide formation from the reduced pyridoindole (**3aH$_2$**) and the pyrroloindole (**3bH$_2$**).

points, we can safely conclude that acetate is eliminated ~4-fold faster from reduced **3b** than from reduced **3a**.

Equation 2 represents the rate law for quinone methide disappearance. This equation was derived by using material balance where reactions occur from an equilibrating mixture of neutral and protonated quinone metide. Both the protonated (k_2 process) and neutral equivalent (k_3 and k_4 processes) react to afford the observed major products shown in Scheme 14. Alternatively, the quinone methide can be protonated at the methide carbon center to afford a proton-trapping product (k_4 process). The k_4 process is expected to parallel the k_3 process on the pH profile because both involve quinone methide protonation along with the participation of hydroxide. Essentially the transition states for both k_3 and k_4 processes consist of neutral quinone methide and water. In fact, the pyridoindole quinone methide traps both water and protons by these respective

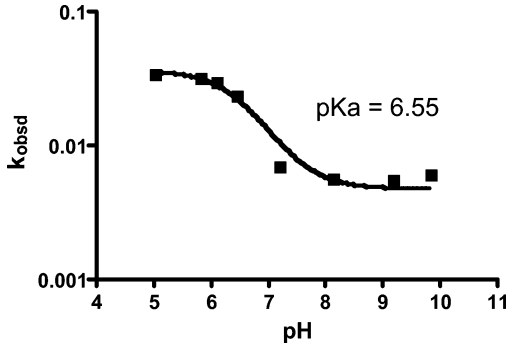

FIGURE 3. pH−rate profile for the decomposition of the pyrroloindole quinone methide.

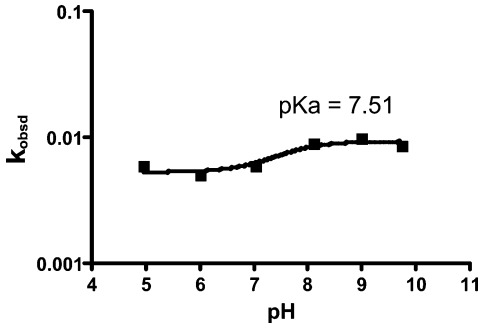

FIGURE 4. pH−rate profile for the decomposition of the pyridoindole quinone methide.

processes only at pH values <p$K_a$where neutral quinone methide is the predominant species. The pyrroloindole quinone methide on the other hand does not exhibit a significant k_4 process.

The pH−rate profiles for the disappearance of the pyrroloindole and pyridoindole quinone methides are shown in Figures 3 and 4, respectively. The data in both profiles were fit to eq 2 generating the constants for the pyrroloindole quinone methide $k_2 = 0.032$ min^{-1}, $K_a = 2.84 \times 10^{-7}$ (p$K_a = 6.55$), $k_3 = 8.98 \times 10^4$ M^{-1} min^{-1} and for the pyridoindole quinone methide $k_2 = 0.006$ min^{-1}, $K_a = 3.5 \times 10^{-8}$ (p$K_a = 7.51$), $k_3 = 1.9 \times 10^4$ M^{-1} min^{-1}. The small inflection point in Figure 4 is significant considering the 1.8-fold difference in k_{obsd} for the high and low pH plateaus and the ±10−15% standard deviation for k_{obsd} values.

The mechanistic interpretation of the pH−rate profiles for quinone methide disappearance (Figures 3 and 4) relied on Hartree−Fock calculations with 6-31G basis sets as well as on product studies. In Figure 5 we show the potential density maps of the protonated and neutral pyridoindole quinone methide with negative charge density in red and positive charge density in blue. Inspection of the methide reacting center of the neutral species reveals a slight negative charge density (yellow-green color). We interpret this observation as the combination of electron release to and electron withdrawal from the methide reacting center (see resonance structures in Figure 5). This result suggests that water does not trap the neutral quinone methide but rather its kinetic equivalent occurs: the hydroxide trapping of the protonated quinone methide. Thus the rate law in eq 2 contains the autoprotolysis constant for water $K_w = 1.5 \times 10^{-14}$ at 30 °C. The numerator expression for hydroxide attack on the protonated quinone methide is $a_H k_3(K_w/a_H)$, which simplifies to $K_w k_3$ in eq 2, where k_3 is the second-order rate constant for hydroxide attack, a_H is the proton activity as measured with a

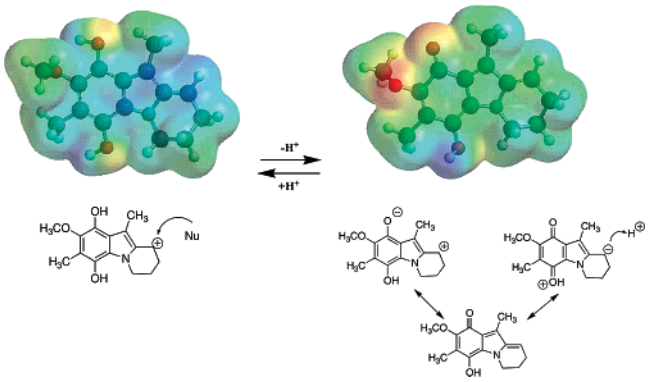

FIGURE 5. Potential density maps for the O-protonated pyridoindole quinone methide and the corresponding neutral species. The charge density color codes are anionic (red), cationic (blue), and neutral (green).

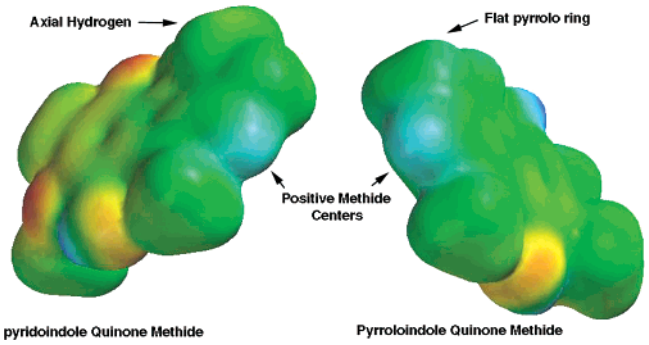

FIGURE 6. Comparison of the potential density maps for the O-protonated pyridoindole and pyrroloindole quinone methides. The charge density color codes are the same as in Figure 5.

pH meter, and K_w/a_H is the hydroxide concentration at a particular a_H value. Thus the k_3 mechanism involves specific acid catalyzed attack of hydroxide. Although the proton concentration decreased, the hydroxide concentration has increased. Therefore the second-order rates of decomposition (k_3) are seen to increase with increasing pH. Consistent with this mechanism, water trapping is the only product observed at pH values above the quinone methide pK_a for both the pyrroloindole and pyridoindole quinone methide.

Proton transfer to the neutral quinone methide can occur either to the slightly electron-rich methide center or to the electron-rich carbonyl oxygen (Figure 5). The former process leads to the proton-trapping product (k_4 in Scheme 15) and the latter process leads to water trapping (k_3 in Scheme 15). Product studies revealed that the pyridoindole quinone methide traps both water and protons by these processes at pH values <pK_a.

The potential density maps illustrated in Figure 6 show that the protonated pyrroloindole and the pyridoindole quinone methides have virtually identical potential density maps. Although the positive potential at the methide centers is nearly identical for both methides, they exhibit differences in rate constants k_0-k_3 and trapping products. The explanation we give for these differences is the greater steric congestion of the fused pyrido ring compared to the relatively flat fused pyrrolo ring. The presence of an axial hydrogen atom in the fused pyrido ring, illustrated in Figure 6, will promote the elimination of acetate from reduced **3a** due to the relief of steric congestion. In contrast, the pyrrolo ring of reduced **3b** eliminates acetate at a 4-fold lower rate constant. Conversely, the pyrroloindole quinone methide traps water and hydroxide with larger rate

TABLE 1. In Vitro Assay Results of Pyridoindole and Pyrroloindole Analogues

compd no.	mid-range log GI_{50} (range)	mid-range log TGI nd range	mid-range log LC_{50} and range
1a	−4.08 (0.06)	−4.01(0.25)	>−4.00 (0)
9	−5.69(3.54)	−5.09(3.59)	−4.52(3.25)
2b	−4.02 (0.06)	>−4.00 (0))	>−4.00 (0)

constants than those observed for the pyridoindole quinone methide. Proton trapping of the pyridoindole methide center can compete with the slowed water trapping affording significant amounts of **20**. Steric congestion can also destabilize biological adducts of the pyridoindole quinone methide. Previously, we reported the preparation of an *N*(7)-pyridoindole adduct of polydG·polydC.[40] Under mild conditions, the N(7) center was eliminated from the pyridoindole adduct to afford **17** and native DNA.

The results enumerated above indicate that pyrroloindole-based reductive alkylating agents are superior to pyrido-based analogues, thus the prevalence of the pyrrolo[1,2-*a*]indole system in naturally occurring bioreductive alkylating agents such as the mitomycins and mitosenes.[21]

Our pH−rate studies and calculated potential density maps indicate that the quinone methide species must be protonated to afford a carbocation before it can trap a nucleophile. Therefore, carbocation pK_a values at or near neutrality are required for nucleophile trapping in a biological system (pH values ∼7.4). Previously, we reported the pK_a for the mitomycin C carbocation−quinone methide equilibrium to be 7.1,[41] a value similar to those obtained from the pH−rate data shown in Figures 3 and 4. In contrast, the pK_a values for a protonated carbonyl oxygen of a ketone or ester usually have negative values. We consider the relatively high pK_a values of 6−8 to be typical for a carbocation−quinone methide equilibrium. The formation of a resonance-stabilized aromatic carbocation is the major reason for these high pK_a values. Electron-rich carbonyl compounds likewise possess positive protonated carbonyl pK_a values. Previously we determined that the pK_a of an *O*-protonated indoloquinone had a value of 1.9 and showed by means of a Bronsted plot that electron-rich protonated quinones can have pK_a values as high as 5.5.[42]

Cell Line Assays. Select pyridoindole and pyrroloindole analogues (**1a**−**d**, **2b**, **2c**, **9**, **10**, **2b**, **17**, **3a**, and **3b**) were screened for cytostatic and cytotoxic activity in human cancer cell line panels (Tables 1 and 2). The cytostatic parameters include GI_{50} and TGI, which are the concentrations of drug required for 50% growth inhibition and total growth inhibition, respectively. The cytotoxic parameter is the LC_{50}, which is the concentration required for 50% cell kill. These data were obtained under the NCI's In Vitro Cell Line Screening Project.[43−45]Also provided in Table 1 is the range value, which represent the log of the maximum concentration difference between the least sensitive and the most sensitive of the 60 cell lines. This range parameter has been used to gain insights into the selectivity of antitumor agents, because it provides a measure of histological specificity.[46] The determinations of log values >−4.00 indicated a lack of activity in the assay results. Thus, we could not achieve the concentration required for a 50% cytostatic or cytotoxic effect even when approaching mM concentration ranges of the compound. Compounds **1b**−**d**, **2c**, and **10** fall into this category and have been left out of Table 1. In Table 2, we show in vitro assays of **17**, **3a**, and **3b** against the six human cancer cell lines. These compounds possess only growth inhibition activity and only the GI_{50} parameter is shown in this table.

The data in Table 1 indicate that both **1a** and **2b** possess low cytostatic activity and no measurable cytotoxic activity. The absence of cytotoxic activity exhibited by these compounds is likely due to their lack of bisalkylation (cross linking) capability. Cross linking is the cytotoxic event of many alkylating agents possessing antitumor activity.[47] Our product studies suggest that the reductive activation of **1a** and **2b** could only result in monoalkylation. The results of product studies outlined in Scheme 14 suggest that compound **1a** could form **17** upon cellular reductive activation. The data in Table 2 indicate that compound **17** possesses low cytostatic activity perhaps due to its nucleophile-trapping capability illustrated in Scheme 13. The reductive activation of **2a** likewise results in a monoalkylation event to afford water-trapping product (Scheme 12).

The presence of an amine substituent on the quinone ring of **1c** results in mainly proton trapping upon reductive activation (Scheme 7). Consistent with this result, the amine substituted analogues **1b**, **1c**, and **1d** lack any detectable cytostatic or cytotoxic activity.

The iminoquinone derivative **9** is the only analogue that possesses a high level of cytostatic and cytotoxic activity along with high cell line specificity (>3 orders of magnitude between resistant and sensitive cell lines). The histological cancers most sensitive to **9** include CNS, melanoma, and breast cancers. COMPARE analysis[43,48] was carried out to provide insights into what might be the molecular target of **9**. The COMPARE analysis correlates mean graph data with known molecular target levels in cell lines and thereby generates hypotheses concerning the agent's mechanism of action. A molecular target is a protein or enzyme that has been measured in the National Cancer Institute's panel of 60 human tumor cell lines. The levels of over one-thousand biologically relevant molecular targets have been determined in these tumor cell lines from measurements of mRNA and enzyme activity levels.[49] Compound **9** appears to target a tyrosine kinase involved in cell division rather than act as an alkylating agent activated by DT-diaphorase. Significantly, the structurally similar quinone analogue **10** lacked cytostatic and cytotoxic activity. Additional studies will be carried out to evaluate **9** as an antitumor agent.

Our kinetic and product studies of **3a** and **3b** correctly predicted the relative activity of the compounds against the six human cancer cell lines listed in Table 2. These studies

(40) Ouyang, A.; Skibo, E. B. *J. Org. Chem.* **1998**, *63*, 1893−1900.
(41) Boruah, R. C.; Skibo, E. B. *J. Org. Chem.* **1995**, *60*, 2232−2243.
(42) Skibo, E. B.; Xing, C. *Biochemistry* **1998**, *37*, 15199−15213.
(43) Paull, D. K.; Shoemaker, R. H.; Hodes, L.; Monks, A.; Scudiero, D. A.; Rubinstein, L.; Plowman, J.; Boyd, M. R. *J. Natl. Cancer Inst.* **1989**, *81*, 1088−1092.
(44) Boyd, M. R. In *Principles and Practices of Oncology* (*PPO updates*), 3rd ed.; DeVita, V. T., Hellman, S., Rosenberg, S. A., Eds.; J. B. Lippincott: Phildelphia, PA, 1989; Vol. 3, pp 1−12.
(45) Boyd, M. R.; Paull, K. D. *Drug Dev. Res.* **1995**, *34*, 91−109.
(46) Xing, C.; Skibo, E. B.; Dorr, R. T. *J. Med. Chem.* **2001**, *44*, 3545−3562.
(47) Kohn, K. W. *Cancer Res.* **1996**, *56*, 5533−5546.
(48) Sausville, E. A.; Zaharevitz, D.; Gussio, R.; Meijer, L.; Louarn-Leost, M.; Kunick, C.; Schultz, R.; Lahusen, T.; Headlee, D.; Stinson, S.; Arbuck, S. G.; Senderowicz, A. *Pharmacol. Ther.* **1999**, *82*, 285−292.
(49) Ross, D. T.; Scherf, U.; Eisen, M. B.; Perou, C. M.; Rees, C.; Spellman, P.; Iyer, V.; Jeffrey, S. S.; Van De Rijn, M.; Waltham, M.; Pergamenschikov, A.; Lee, J. C. E.; Lashkari, D.; Shalon, D.; Myers, T. G.; Weinstein, J. N.; Botstein, D.; Brown, P. O. *Nat. Genet.* **2000**, *24*, 227−235.

TABLE 2. In Vitro Assay Results for 18, 3a, and 3b in Six Human Cancer Cell Lines

parameter	BxPC-3 pancreas	MCF-7 breast	SF-268 CNS	H460 NSC lung	KM20L2 colorectal	DU-145 prostrate
17 log GI_{50}	−4.14	−4.75	−4.36	−4.81	−4.58	−4.36
3a log GI_{50}	>−4	>−4	>−4	>−4	>−4	>−4
3b log GI_{50}	−4.8	−4.95	>−4	−4.95	>−4	−4.96

determined that the pyridoindole quinone methide formed upon reduction of **3a** is a poor nucleophile trap with a tendency to eliminate the nucleophile. Consistent with these findings, **3a** lacked both cytostatic and cytotoxic activity. In contrast, the pyrroloindole quinone methide derived from reduction of **3b** is an excellent nucleophile trap and accordingly this compound exhibits significant cytostatic activity (Table 2).

Conclusions

In the present study, we investigate pyrido[1,2-*a*]indole- and pyrrolo[1,2-*a*]indole-based quinones capable of forming quinone methide and vinyl quinone species upon reduction and leaving group elimination. Our goals were to determine the influence of the 6-membered pyrido and the 5-membered pyrrolo fused rings on the formation and fate of these species as well as on their cytostatic and cytotoxic activity. Our efforts were aided by the development of a new technique for rapid quinone reduction to the hydroquinone in a Thunberg (anaerobic) cuvette. As result, it was possible to carry out direct kinetic studies of quinone methide formation and fate by using Spectral Global Fitting.[20] The postulate made at the outset of this study was that reactive species derived from the 6-membered pyrido ring analogues would be less reactive than those derived from the 5-membered pyrrolo ring analogues. The presence of axial hydrogens in the fused pyrido ring, in contrast to the relatively flat fused pyrrolo ring, was the basis for this postulate.

Kinetic studies of quinone methide formation and fate led to the following conclusions: The pK_a of the protonated quinone methide is near neutrality, only protonated quinone methide traps nucleophiles, and only neutral quinone methide traps protons. Typically carbonyl oxygen protonations are associated with pK_a values <0 because the resulting cations are often not stable. In contrast, *O*-protonated quinone methides are resonance stabilized aromatic cations. Potential density maps show that the methide reacting center has positive charge density only upon protonation. Therefore, nucleophile trapping by a quinone methide requires a preequilibrium *O*-protonation. Thus the pK_a values of *O*-protonated quinone methides near neutrality are largely responsible for the biological activity of reductive alkylating agents. Potential density maps also show that the reacting center of the neutral quinone methide is slightly anionic (yellow color). As a result, proton transfer to this center competes with proton transfer to the carbonyl oxygen. Proton trapping only occurs at pH values at or below the *O*-protonated quinone methide pK_a. Proton trapping product concentration vs pH data has been used to estimate *O*-protonated quinone methide pK_a values.[41] The Global Fitting studies described in this report have made it possible to measure these pK_a values directly.

The comparative kinetic studies of the pyridoindole and the pyrroloindole quinone methides led to our conclusion that the former are unsuitable for alkylating agent design. The reason is that the trapping of a biological nucleophile by a pyridoindole quinone methide would be reversible due to steric congestion. Our experimental findings showed that the fused pyrido ring promotes quinone methide and vinyl quinone formation but slows nucleophile trapping compared to a fused pyrrolo ring. These findings are consistent with the presence of axial hydrogen atoms in the fused pyrido ring that result in more steric congestion compared to the relatively flat fused pyrrolo ring. The elimination of a large biological nucleophile (DNA) from a pyrroloindole system was demonstrated by a previous study.[40]

Human cancer cell line cytostatic and cytotoxic studies validated our conclusion that pyridoindole quinone methides are unsuitable for alkylating agent design. The pyrroloindole analogue **3b** possessed cytostatic activity but the pyridoindole analogue **3a** was inactive. Likewise, the other pyridoindole analogues were inactive with some exceptions. Compound **17** possesses modest cytostatic activity perhaps due to alkylation reactions involving the quinone ring. Compound **9** is the only analogue that possesses high levels of both cytostatic and cytotoxic activity. The mechanism of activity likely involves kinase cellular targets rather than alkylation reactions.

Experimental Section

Select compounds were screened in the National Cancer Institute's 60-cell line screen.[43,50] Mean graph results were then analyzed with COMPARE online (http://itbwork.nci.nih.gov/PublicServer/jsp/Form_Upload.jsp).[43,48] Syntheses of the compounds leading to series **1**, in vitro studies, kinetic studies, and calculations were carried out as outlined below. The syntheses of series **2** and **3** and the product isolation studies are described in the Supplemental Information.

6,7,8,9-Tetrahydro-3,10-dimethyl-2-methoxy-1-nitropyrido-[1,2-*a*]indole-9-ol (5). Sodium borohydride (0.5 g, 13.2 mmol) was added portionwise to a solution of 6,7,8,9-tetrahydro-2-methoxy-3,10-dimethyl-1-nitro-9-oxo-pyrido[1,2-*a*]indole (**4**)[12] (1.2 g, 4.16 mmol) in 70 mL of methanol cooled to 0 °C. After addition was completed, the reaction mixture was stirred at room temperature for 25 min. The mixture was concentrated in vacuo to dryness and the residue was suspended in water (100 mL) and extracted with methylene chloride (3 × 50 mL). The combined organic layers were dried over Na_2SO_4, filtered, and evaporated. The remaining solids were purified by filtration over pad of silica gel with methylene chloride as the eluent. Compound **5** was crystallized from methylene chloride/hexane to afford a yellow crystalline solid: 1.1 g (91%) yield; mp 161−162 °C; IR (KBr pellet) 3408, 3030, 2924, 2866, 1521, 1444, 1371, 1276, 1238 cm^{-1}; ^1H NMR ($CDCl_3$) δ 7.17 (1H, s), 5.15 (1H, t, $J = 3.9$ Hz), 4.22 (1H, m), 3.85 (3H, s), 3.77 (1H, m), 2.43 (3H, s), 2,40 (1H, m), 2.20 (1H, m), 2.17(3H, s), 2.02 (1H, m); HREI MS *m*/*z* calcd for $C_{15}H_{18}N_2O_4$ 290.1267, found 290.1277. Anal. Calcd for $C_{15}H_{18}N_2O_4$: C, 62.06; H, 6.25; N, 9.65. Found: C, 61.90; H, 6.24; N, 9.46.

6,7-Dihydro-2-methoxy-3,10-dimethyl-1-nitropyrido[1,2-*a*]indole (6). To a stirred solution of **5** (500 mg, 1.8 mmol) in dry methylene chloride under nitrogen and cooled to 0 °C was added 345 mg (2.8 mmol) of DMAP, followed by 300 μL (3.8 mmol) of methanesulfonyl chloride. The reaction was stirred for 1 h while being cooled with an ice bath, and then stirring was continued at room temperature for 48 h. Solid byproducts were removed by filtration, the filtrate was evaporated under reduced pressure, and

(50) Strumberg, D.; Pommier, Y.; Paull, K.; Jayaraman, M.; Nagafuji, P.; Cushman, M. *J. Med. Chem.* **1999**, *42*, 446−457.

then the crude product was purified by flash silica gel chromatography with methylene chloride as the eluent. Compound **6** was crystallized from methylene chloride/hexane to afford the product as a yellow crystalline solid: 320 mg (68%) yield; mp 126−127 °C; IR (KBr pellet) 3001, 2920, 1521, 1462, 1325, 1151, 1030, 754 cm^{-1}; ^1H NMR ($CDCl_3$) δ 7.12 (1H, s), 6.66 (1H, doublet of triplets, J = 2.1, 6 Hz), 6.07 (1H, m), 4.04 (2H, t, J = 6.9 Hz), 3.86 (1H, s), 2.66 (2H, m), 2.43 (3H, s), 2.12 (3H, s); HREI MS m/z calcd for $C_{15}H_{16}N_2O_3$ 272.1161, found 272.1153. Anal. Calcd for $C_{15}H_{16}N_2O_3$: C, 66.16; H, 5.92; N, 10.29. Found: C, 66.20; H, 5.94; N, 10.25.

6,7,8,9-Tetrahydro-2-methoxy-3,10-dimethyl-1-nitropyrido-[1,2-*a*]indole-*cis*-8,9-diol (7). Compound **6** (500 mg, 1.8 mmol) was added to a mixture consisting of a 0.8 mL solution of osmium tetroxide (2.5% in 2-methyl-2-propanol), 240 mg of *N*-methylmorpholine *N*-oxide dihydrate, and 30 mL of *t*-BuOH/THF/H_2O (3:1:1). The reaction mixture was then stirred at 25 °C for 1 h. Aqueous saturated $NaHSO_3$ was then added to the reaction mixture which was stirred for 1 h; this mixture was then extracted with CH_2Cl_2 (3 × 50 mL). The combined organic layers were dried over Na_2SO_4, filtered, and evaporated under reduced pressure. Column chromatography of the crude product was carried out on silica gel with CH_2Cl_2/MeOH (99:1) as the eluent. Compound **7** was crystallized from methylene chloride/hexane to afford the product as a light yellow crystalline solid: 510 mg (89%) yield; mp ≥165 °C dec; IR (KBr pellet) 3296, 3020, 2922, 1743, 1672, 1525, 1361, 1103, 1030 cm^{-1}; ^1H NMR (DMSO-d_6) δ 7.45 (1H, s), 5.15 (1H, d, J = 5.7 Hz), 4.96 (1H, d, J = 5.4 Hz), 4.79 (1H, t, J = 3.9 Hz), 4.23 (1H, m), 3.87 (2H, m), 3.75 (3H, s), 2.38 (3H, s), 2.25 (1H, m), 2.02 (3H, s), 1.91(1H, m); HREI MS m/z calcd for $C_{15}H_{18}N_2O_5$ 306.1216, found 306.1206. Anal. Calcd for $C_{15}H_{18}N_2O_5$: C, 58.82; H, 5.92; N, 9.15. Found: C, 58.73; H, 5.80; N, 9.07.

6,7,8,9-Tetrahydro-*cis*-8,9-dihydroxy-2-methoxy-3,10-dimethylpyrido[1,2-*a*]indole-1,4-dione (8). 8 was prepared by the following two-step process:

The product obtained above (**7**, 300 mg, 0.98 mmol) was catalytically reduced for 45 min in methanol under 50 psi of H_2 employing 100 mg of 5% Pd on carbon as catalyst. After complete reduction, the catalyst was removed by filtration through Celite and the filtrate concentrated to a residue. No attempt was made to purify the reactive amino diol product.

This product was dissolved in 2 mL of MeOH to which was added 30 mL of 0.1 M monobasic potassium phosphate buffer held at pH 3.20. To this solution was added a solution consisting of 4 g of Fremy salt in 100 mL of the same phosphate buffer. The reaction mixture was stirred at room temperature for 45 min and then extracted with 4 × 50 mL of chloroform. The dried extracts (Na_2SO_4) were concentrated and the residue purified with flash column chromatography on silica gel employing CH_2Cl_2/MeOH (97:3) as the eluent. Two fractions were collected: The major compound (**8**) was crystallized from methylene chloride/hexane to afford a light orange crystalline solid: 167 mg (58%); mp ≥170 °C dec; IR (KBr pellet) 3400, 3296, 3010, 2930, 1601, 1639, 1502, 1446, 1325, 1101, 1001 cm^{-1}; ^1H NMR (DMSO-d_6) δ 5.16 (1H, d, J = 5.4 Hz), 4.96 (1H, d, J = 5.4 Hz), 4.64 (1H, t), 4.43 (1H, m), 4.06 (1H, m), 3.85 (3H, s), 3.81 (1H, m), 2.23 (3H, s), 2.12 (1H, m), 1.82 (3H,s), 1.81 (1H, m); HREI MS m/z calcd for $C_{15}H_{17}NO_5$ 291.1107, found 291.1101. Anal. Calcd for $C_{15}H_{17}NO_5$: C, 61.85; H, 5.88; N, 4.81. Found: C, 61.64; H, 5.83; N, 4.77. The minor product 6,7,8,9-tetrahydro-*cis*-8,9-dihydroxy-2-methoxy-3,10-dimethylpyrido[1,2-*a*]indole-1-imino-4-one (**9**) was crystallized from methylene chloride/hexane to afford the product as a light yellow crystalline solid: 57 mg (20%); mp ≥166 °C dec; IR (KBr pellet) 3246, 2939, 1751, 1637, 1444, 1296, 1217,-1095, 1001 cm^{-1}; ^1H NMR (DMSO-d_6) δ 10.76 (1H, S), 5.10 (1H, d, J = 5.4 Hz), 4.93 (1H, d, J = 5.4 Hz), 4.68 (1H, broad), 4.55 (1H, m), 4.09 (1H, m), 3.83 (2H, m), 3.72 (3H, s), 2.33 (3H, s), 2.16 (2H, m), 1.89 (3H, s), 1.84 (1H, m); HREI MS m/z calcd for $C_{15}H_{18}N_2O_4$ 290.1267, found 290.1277. Anal. Calcd for $C_{15}H_{17}NO_5$: C, 62.06; H, 6.25; N, 9.65. Found: C, 61.85; H, 6.35; N, 8.91.

***cis*-8,9-Diacetoxy-6,7,8,9-tetrahydro-2-methoxy-3,10-dimethylpyrido[1,2-*a*]indole-1,4-dione (1a).** To a stirred solution of **8** (200 mg, 0.68 mmol) in 15 mL of dry methylene chloride under nitrogen and cooled to 0 °C was added 50 mg of DMAP, followed by 0.7 mL of acetic anhydride dropwise. The reaction mixture was stirred for 10 min at room temperature, and then solvent was evaporated. Crude product was purified by flash silica gel chromatography with methylene chloride as the eluent. Compound **1a** was crystallized from methylene chloride/hexane to afford the product as a light orange crystalline solid: 215 mg (83%); mp 185−186 °C; IR (KBr pellet) 3010, 2947, 1737, 1643, 1502, 1369, 1248, 1024 cm^{-1}; ^1H NMR ($CDCl_3$) δ 6. 37 (1H, t), 5.24 (1H, m), 4.82 (1H, m), 4.11(1H, m), 4.00 (3H, s), 2.46 (1H, m), 2.22 (3H, s), 2.12 (1H, m), 2.09 (3H, s), 2.05 (3H, s), 1.94 (3H, s); HREI MS m/z calcd for $C_{19}H_{21}NO_7$ 375.1318, found 375.1332. Anal. Calcd for $C_{19}H_{21}NO_7$: C, 60.79; H, 5.64; N, 3.73. Found: C, 60.90; H, 5.59; N, 3.74.

***cis*-8,9-Diacetoxy-2-aziridinyl-6,7,8,9-tetrahydro-3,10-dimethylpyrido[1,2-*a*]indole-1,4-dione (1b).** To a stirred solution of **1a** (50 mg, 0.13 mmol) in 10 mL of methanol cooled to 0 °C was added 300 μL of aziridine dropwise. Reaction was stirred for 1.5 h at room temperature, and then the solvent was evaporated. Crude product was purified by flash silica gel chromatography (methylene chloride/ MeOH 98:2) as the eluent. Compound **1b** was crystallized from methylene chloride/hexane to afford the product as a light yellow crystalline solid: 38 mg (74%); mp 191−193 °C; IR (KBr pellet) 2947, 1737, 1643, 1369, 1249, 1024 cm^{-1}; ^1H NMR ($CDCl_3$) δ 6.36 (1H, d, J = 3.3 Hz), 5.25 (1H, m), 4.90 (1H, m), 4.16 (1H, m), 2.49 (1H, m), 2.28 (4H, s), 2.22 (3H, s), 2.10 (3H, s), 2.09 (1H, m), 2.09 (3H, s), 2.04 (3H, s); MALDI m/z calcd for $C_{20}H_{23}N_2O_6$ (M + 1) 387.1551, found 387.149.

***cis*-8,9-Dihydroxy-6,7,8,9-tetrahydro-2-(2-methoxyethylamino)-3,10-dimethylpyrido[1,2-*a*]indole-1,4-dione (10).** To a stirred solution of **8** (200 mg, 0.68 mmol) in 30 mL of methanol was added 300 μL of 2-methoxyethylamine dropwise. Reaction was stirred overnight at room temperature, and then product was filtered off. The crude product was crystallized from methanol to give **10** as a magenta solid: 185 mg (80%); mp ≥191 °C dec; IR (KBr pellet) 3331, 3254, 2922, 1660, 1599, 1504, 1294, 1011, 952 cm^{-1}; ^1H NMR (DMSO-d_6) δ 6.11 (1H, NH), 5.04 (1H, d, J = 5.4 Hz), 4.90 (1H, d, J = 5.4 Hz), 4.62 (1H, m), 4.45 (1H, m), 3.99 (1H, m), 3.80 (1H, m), 3.63 (2 H, m), 3.48 (2H, m), 3.26 (3H, s), 2.20 (3H,s), 2.07 (1H,m), 1.93 (3 H, s), 1.83(2H, m); HREI MS m/z calcd for $C_{17}H_{22}N_2O_5$ 334.1529, found 334.1540. Anal. Calcd for $C_{17}H_{22}N_2O_5$ C, 61.07; H, 6.63; N, 8.38. Found: C, 61.08; H, 6.61; N, 8.26.

***cis*-8,9-Diacetoxy-6,7,8,9-tetrahydro-2-(2-methoxyethylamino)-3,10-dimethylpyrido[1,2-*a*]indole-1,4-dione (1c).** To a stirred solution of **10** (100 mg, 0.30 mmol) in 50 mL of dry methylene chloride cooled to 0 °C was added 35 mg of DMAP, followed by dropwise addition of 0.5 mL of acetic anhydride. The reaction was stirred for 45 min at room temperature and then the solvent was evaporated in vacuo. The residue was suspended in 100 mL of water and the product was extracted with ethyl acetate (4 × 50 mL). The combined organic layers were dried over Na_2SO_4, filtered, and evaporated. Crude product was purified by flash silica gel chromatography with methylene chloride/ MeOH (96:4) as the eluent. Compound **1c** was crystallized from methylene chloride/hexane to afford a magenta solid: 100 mg (80%) yield; mp 147−148 °C; IR (KBr pellet) 3323, 3010, 2926, 1737, 1666, 1602, 1508, 1248, 1107 $cm^{-1;}$ ^1H NMR (DMSO-d_6) δ 6.25 (1H, d, J = 4.8 Hz), 6.21 (1H, NH), 5.25 (1H, doublet of triplets, J = 3.3, 4.8 Hz), 4.75 (1H, m), 4.17 (1H, m), 3.67 (2H, m), 3.49 (2H, m), 3.27 (3H. s), 2.28 (1H, m), 2.10 (3H, s), 2.08 (1H, m), 2.06 (3H, s), 1.99 (3H, s), 1.95 (3H, s); HREI MS m/z calcd for $C_{21}H_{26}N_2O_7$ 418.1740, found 418.1736. Anal. Calcd for $C_{21}H_{26}N_2O_7$: C, 60.28; H, 6.26; N, 6.69. Found: C, 60.24; H, 6.25; N, 6.60.

***cis*-8,9-Dihydroxy-6,7,8,9-tetrahydro-2-(2-methoxyethylamino)-3,10-dimethylpyrido[1,2-*a*]indole-1,4-dione Carbonic Acid Ester (1d).** Triphosgene (100 mg, 0.33 mmol) in dry methylene chloride was added dropwise to a stirred solution of **10** (100 mg, 0.3 mmol) in 0.5 mL of dry pyridine and 10 mL of dry CH_2Cl_2 cooled to 0 °C. The reaction was stirred at room temperature and the reaction progress was monitored by thin layer chromatography. After 5 min, the solution was diluted with water and the two phases were separated and the aqueous phase was extracted with CH_2Cl_2 (3 × 5 mL). The combined organic phases were dried (Na_2SO_4) and concentrated to a residue, which was purified by flash chromatography on silica gel with CH_2Cl_2 as the eluent. The isolated carbonate was recrystallized from CH_2Cl_2/hexane: 60 mg (56%) yield; mp ≥159 °C dec; IR (KBr pellet) 3338, 2926, 1786, 1655, 1599, 1508, 1122, 1024 cm^{-1}; ^1H NMR ($CDCl_3$) δ 6.05 (1H, NH), 5.84 (1H, d, J = 8.4 Hz), 5.19 (1H, m), 5.13 (1H, t, J = 4.5 Hz), 4.17 (1H, m), 3.72 (2H, m), 3.57 (2H, m), 3.38 (3H, s), 2.42 (1H, m), 2.32 (3H, s), 2.07 (1H, m), 2.05 (3H, s); HREI MS *m*/*z* calcd for $C_{18}H_{20}N_2O_6$ 360.1321, found 360.1338. Anal. Calcd for $C_{18}H_{20}N_2O_6$: C, 59.99; H, 5.59; N, 7.77. Found: C, 58.64; H, 5.47; N, 7.38.

The NCI in Vitro Screening Procedures. Compounds were tested against all cell lines included in the 60 cell line panel. All cell lines are inoculated onto a series of standard 96-well microtiter plates that consists of cell suspensions that were diluted according to the particular cell type (expected target cell density 5000−40000 cells per well based on cell growth characteristics). Inoculates were preincubated for a period of 24 h at 37 °C in the absence of any test compound. Each test compound was added in 100 μL aliquots to the microtiter plate wells and evaluated at five 10-fold dilutions with a high concentration of 10^{-4} M. Incubation with test compounds lasted 48 h in an atmosphere of 5% carbon dioxide with 100% humidity. The cells are assayed by the sulforhodamine B procedure. Afterward, a plate reader was used to read the optical densities, and a computer processed the optical densities into the special concentration parameters GI_{50}, TGI, and LC_{50}.

Kinetic Studies of Quinone Methide Formation and Fate. The stock solutions of **3a** and **3b** were prepared by diluting 4 to 5 mg in a 5 mL volumetric flask with dry dimethyl sulfoxide (DMSO) to afford solutions with concentrations of 2.5 to 3.3 mM. All kinetic studies were carried out with buffers prepared from doubly distilled water. Final concentrations of the **3a** and **3b** in reaction mixtures ranged from 83 to 110 μM. DMSO concentrations in reaction mixtures were kept <2% to minimize solvent effects. The following buffer systems were used to hold pH: 1 M acetate buffer (pH 4 to 6.5), 0.2 M phosphate buffer (pH 6.5 to 8.5), and 0.2 M borate buffer (pH 7.5 to 10). All buffers were maintained at an ionic strength (μ) of 1.0 with KCl. The temperature of all the kinetic measurements was maintained at 30.0 ± 0.3 °C with circulating water from a thermostatic water bath.

The reactions were carried out in Thunberg cuvettes in the following way: To the bottom port of the Thunberg was added 2.8 mL of buffer and 100 μL of a sonicated suspension consisting of 50 mg of 5% Pd on carbon in 10 mL of water. The amount of catalyst added to the bottom port was 0.5 μg. To the top port of the Thunberg cuvette was added 100 μL of the DMSO stock of **3a** or **3b**. The cuvette was sealed with Apiazon L grease and Teflon tubes from a hydrogen source were threaded into the top and bottom ports. After the ports were purged with hydrogen gas for 5 min, the cuvette was sealed and equilibrated at 30 °C in the thermostated spectrometer. We started the reaction by combining the top and bottom ports. Reactions were monitored between 240 and 600 nm with a UV−visible spectrophotometer equipped with Spectral Global Fitting software. The reaction times varied from 400 to 600 min depending on the pH of the reaction. When the reactions were complete the pH of the samples was taken and recorded for use on the pH−rate profile.

Calculations. The absorbance vs time vs wavelength surfaces obtained as described above was fit with Global fitting software.[20,38] These fits provide first-order and two consecutive first-order rate constants along with intermediate spectra, if any. Log k_{obsd} vs pH data were fit with Graph Pad Prism 3 software, which was also used to generate the solid curve shown in pH−rate profiles. Electrostatic potential maps were obtained with Hartree−Fock calculations that were carried out with the 3-21G(*) basis set.[36]

Acknowledgment. We thank the Arizona State University College of Liberal Arts and Sciences for their generous support and Jean-Charles Chapuis for running the assays shown in Table 2.

Supporting Information Available: Proton NMR spectra of reported compounds and ^{13}C NMR spectra of select compounds along with the experimental details for the syntheses of compound series **2** and **3**. This material is available free of charge via the Internet at http://pubs.acs.org.

JO070866O